Received 10 December 2015; revised 6 January 2016; accepted 6 January 2016. Date of publication 19 January 2016; date of current version 23 February 2016.
The review of this paper was arranged by Editor A. G. U. Perera.

Digital Object Identifier 10.1109/JEDS.2016.2516026

A 1 μm-Pitch Quanta Image Sensor Jot Device With Shared Readout

JIAJU MA (Student Member, IEEE), LEO ANZAGIRA (Student Member, IEEE), AND ERIC R. FOSSUM (Fellow, IEEE)

Thayer School of Engineering, Dartmouth College, Hanover, NH 03755, USA

CORRESPONDING AUTHOR: E. R. FOSSUM (e-mail: eric.r.fossum@dartmouth.edu)

This work was supported by Rambus, Inc.

ABSTRACT Characterization of a 1 μm-pitch, four-way shared readout quanta image sensor jot device is reported. The jot device achieved 0.48e− r.m.s. read noise with 230 μV/e- conversion gain. Quantum efficiency, dark current, and lag results are discussed. Cross-talk was investigated using TCAD simulation and the results are analyzed.

INDEX TERMS Quanta image sensor, CMOS image sensor, jot device, pixel size shrinking, photon counting, low read noise.

I. INTRODUCTION

After the CMOS image sensor (CIS) was invented, pixels have generally followed the CMOS process scaling trend [1]. The minimum size of one pixel has been reduced by over 30x, to the current 1-2μm range, which is in the sub-diffraction-limit (SDL) regime. As discussed in [2], SDL pixels cannot improve the effective image resolution, and typically lead to poorer image quality because of lower dynamic range and worse low-light signal-to-noise ratio (SNR). The Quanta Image Sensor (QIS) was proposed to take advantage of the shrinking pixel size and realize better image quality by counting each single incident photon [3]. In the QIS concept there may be a billion specialized tiny pixels that are called jots. The noise floor of a jot needs to be in the deep sub-electron regime, preferably 0.15e- r.m.s. or less, so that single photoelectrons can be sensed [4], [5]. The jots will be scanned at a high frame rate, and in a single-bit QIS, each jot will output a binary signal based on the presence or absence of at least one photoelectron. The output image pixels are created from the binary jot data by image processing [6]. The size of a jot needs to be very small, e.g., 200nm-500nm, so that the likelihood that one jot is hit by multiple photons can be reduced. Taking advantage of the small full-well capacity (FWC) needed for a jot, e.g., 1-100e-, jot size shrink has more flexibility than that of a conventional 4T pixel with a pinned photodiode (PPD), but like in pixel shrink, it is challenging to maintain high quantum efficiency and low cross-talk with small device size. The invention of shared readout (SRO) technique has greatly helped improving pixel performance with shrinking size in CIS [7]. Based on this technology, several photosensitive elements, typically a pinned photodiode with a transfer gate, share "active" pixel components. With the shared structure, the fill-factor can be increased while the average size of each pixel becomes smaller. CIS pixels with pitch size in the 1μm range have been realized based on the shared readout structure [8]–[10].

A pump-gate (PG) photon-counting jot device was designed and reported by our group [11], [12]. The device features a distal floating diffusion (FD) that has nearly no capacitive coupling to the transfer gate (TG). Read noise as low as 0.22e- r.m.s. read noise with 430μV/e- conversion gain and 210e- FWC was demonstrated. Photoelectron counting capability was proven with this device at room temperature using just one single CDS read and without avalanche gain. The reported PG jot device uses a non-shared readout structure, with 1.4μm pitch size ($2\mu m^2$).

Since then, other photon-counting pixel structures that do not use avalanche gain have been reported. For example, a more conventional CIS pixel was demonstrated with read noise of 0.27e- r.m.s. at a conversion gain of 220μV/e- at -10C using $63\mu m^2$ pixel size and 1,500e- FWC [13].

In this paper, a 4-way shared readout PG jot device with 1μm pitch size is reported. The SRO device takes advantage

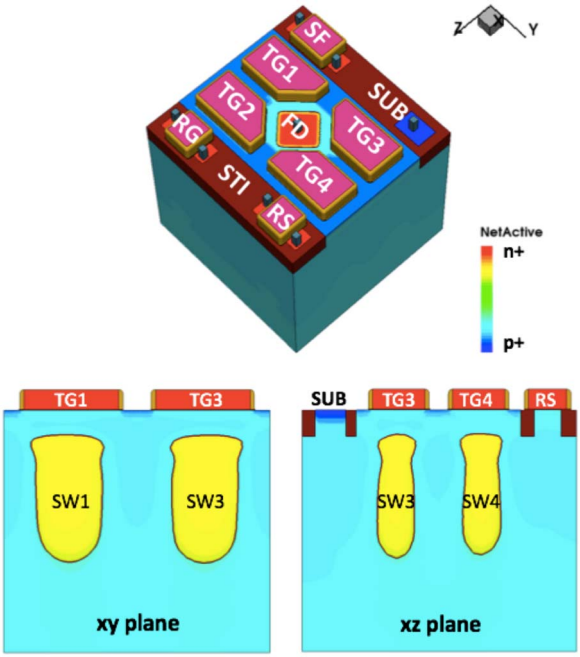

FIGURE 1. **Doping profile of the shared readout jot device from TCAD tools. The simulation reflects the TSMC 65nm BSI CIS process. The top is the 3D model, and the XY and XZ cut-planes are shown on the bottom.**

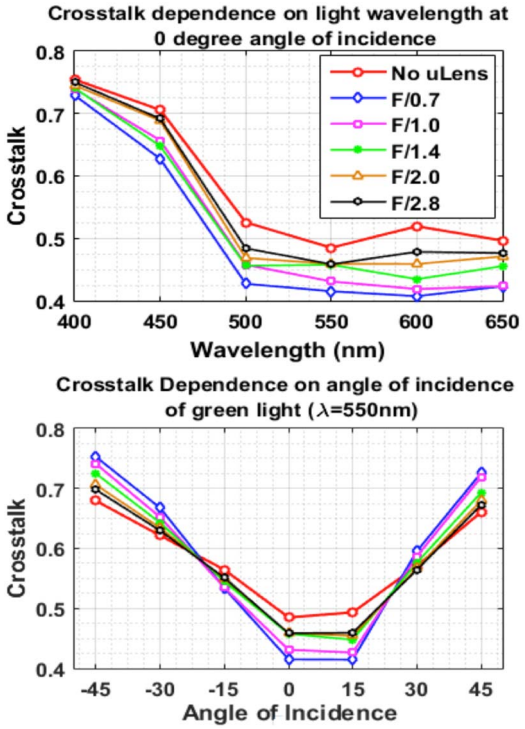

FIGURE 2. **TCAD simulation results of crosstalk with different wavelength (top) and different incident angle (bottom). Crosstalk is given by the ratio of signal in neighboring jots to total signal in all jots in the 3x3 jot array.**

of the distal FD of the pump-gate jot so that sharing the FD does not reduce CG due to increased TG coupling capacitance. However, the CG was reduced due to other factors yielding limited photon-counting capability for this design iteration. The paper will also discuss issues related to jot device shrink and performance related to small pitch size, such as cross-talk, dark current and quantum efficiency.

II. DEVICE DESCRIPTION AND CROSS-TALK SIMULATION

The concept of pump gate structure is described in [14]. Like the previously reported non-shared PG jots, the SRO jot device was fabricated in the TSMC 65nm BSI CIS process with just a few implant modifications. Color filters and microlenses were not fabricated. The layout of this SRO jot can be found in [14] and the approximate doping profile is shown in Fig. 1. The process recipe was not optimized to minimize crosstalk. The blue light response of the jot is relative low in this design iteration since the photodiode doesn't extend deep enough for light generated close to the backside to be collected. The reason for this is that the SRO jot used the same implant conditions as the non-shared jots in this iteration, and the implants were optimized for the larger non-shared jots. Future design iterations can improve carrier collection by modifying the implant dose and energy of the deep n-well of the photodiode.

As discussed in [11], photoelectrons in the storage well (SW) will be transferred to FD in a two-step pump transfer. Four jots are configured in a 2x2 group and share one FD in the center. Photoelectrons accumulated in the four SWs are transferred to the FD in sequence. A deep p-well is used to separate the four jots, and to reduce cross-talk within the four jots. The deep p-well also helps deflect photoelectrons away from FD, which improves the quantum efficiency. As the size of the jots is scaled down, the width of deep p-well separation will also be reduced accordingly, which will lead to higher cross-talk within the SRO-jots. To reduce the impact of higher SRO jot cross-talk, one single color filter and micro-lens could be shared by four jots. This approach can also relieve the requirements of fabrication process. On the other hand, to reduce the crosstalk between SRO-jot groups, the deep trench isolation (DTI) technique can be used in future jot devices [10].

The crosstalk in the actual jot device could not be characterized due to the relatively small jot size and limitations of our current characterization set-up. However, by means of TCAD simulation tools, the jot's crosstalk dependence on various factors can be investigated. Crosstalk here refers to the phenomenon where light incident over one jot/pixel results in the generation of signal in neighboring jots/pixels.

For this investigation, a set of 3x3 (9) jots was simulated. The central jot is a corner of a 2x2 SRO group, and 3 of the remaining 8 simulated jots belong to the same group. The other 5 belong to neighboring groups. All jots were covered by a metal shield except the middle jot. Ideally, only this central jot would produce a signal when the array is exposed to illumination, however, as a result of optical and electrical crosstalk, neighboring jots will produce

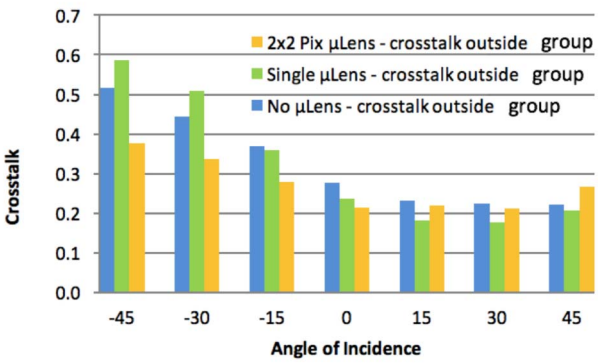

FIGURE 3. **TCAD simulation results of crosstalk from 2x2 jot groups with different microlens setups. Crosstalk here is given by the ratio of the sum of signal in jots outside of the 2x2 jot group to the total signal in all jots.**

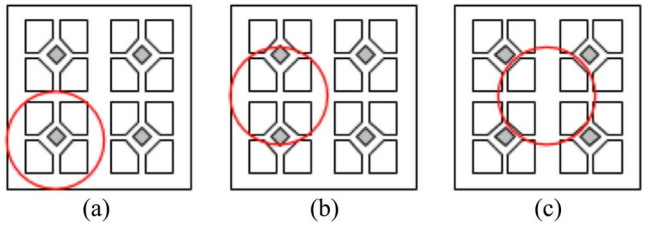

FIGURE 4. **4-way shared jots – the red circle illustrates a microlens placed over a group of 2x2 jots. Microlens may be placed over jots which share the same floating diffusion as in (a) or jots from different shared groups as in (b) and (c).**

some signal. The crosstalk is calculated as the ratio of signal in the neighboring jots to the total number of photoelectrons in all jots.

Simulations were performed for different light wavelengths and angles of incidence. In these simulations, the impact of a microlens was tested by simulating arrays both with and without a microlens over jots. For tests where a microlens is used, the microlens f-number dependence of crosstalk was also explored. Different f-number microlens are simulated in TCAD by varying the radius of curvature of the lens. From simulation results in Fig. 2, it can be seen that blue wavelengths, 400 and 450 have high crosstalk values. This is expected since blue light generates photoelectrons very close to the backside which are not readily collected by the current design iteration, and instead may be lost by diffusion to neighboring jots or recombination. Microlenses improve crosstalk, but only very low f-number microlenses significantly minimize crosstalk at normal incidence. At larger incidence angles ($\sim 30^{o} - 45^{o}$), this trend is reversed with microlenses causing increased crosstalk since the light converges to a region outside of the pixel at such angles. A minimum value of 41% crosstalk is recorded for light of wavelength 550nm.

Since the light focusing ability of microlenses for visible light wavelengths is minimized as jot sizes decrease to the sub-micron level [15], another aspect of this simulation considered the effect of patterning a single microlens over 2x2 SRO-jots groups. Fig. 4 shows different configurations of 2x2 pixel regions with a single microlens. In figure 4a, the microlens is placed over 2x2 region of jots which share the same floating diffusion. In (b) and (c), the microlens is disposed over jots from different groups.

The same 3x3 jot array is used and only middle jot is exposed. However, the crosstalk is now calculated as ratio of photoelectrons in neighboring jots outside of the 2x2 jot group to the total number of photoelectrons. Crosstalk between jots in a single 2x2 jot group is ignored since the outputs of the four jots in the group are summed to generate a single image pixel value.

Fig. 3 compares the crosstalk from 2x2 pixel groups in scenarios where a single microlens is used over the group of jots as shown in Fig. 4a to scenarios where no microlenses are used or where each jot in the group has its own microlens. For this comparison, f/0.7 microlenses are used. There is asymmetry in the crosstalk behavior in going from negative to positive angles of incidence because of the relative position of the middle jot in the SRO-group. For positive angles, the light incident over the middle pixel is still collected by pixels belonging to the same group as the middle pixel resulting in low crosstalk. For negative angles, the light is focused outside the group resulting in the high crosstalk level.

For small angles and large positive angles, most of the crosstalk is within the group for all cases. However, it can be seen that there's a significant advantage to using a single microlens over a 2x2 group for large negative incidence angles (-30 and -45). The crosstalk to jots outside the group at these larger angles is minimized to below 40% using this shared microlens configuration. In contrast, when the conventional 1 microlens/jot configuration is used, crosstalk to jots outside the group increases to 59%. Similar results were obtained for the other two configurations of the shared microlens shown in Figs. 4b and 4c.

While crosstalk is certainly an issue with SDL pixels and can be improved by use of DTI, better doping profiles, and advanced optical structures, for the QIS, where an entire SRO group may be under a single color filter and microlens, cross-talk is less critical. Exactly which jot a photoelectron arrives in is not as important as being able to count it accurately, especially since the purpose of small SDL jot pitch is improving flux capacity, not optical resolution. Crosstalk between groups will remain an issue.

III. CHARACTERIZATION

A. SIGNAL READ OUT CHAIN

A detailed discussion of the readout chain can be found in [12]. As a brief review, there are twenty (20) 32x32 jot arrays with design variations, and four among them are SRO jots. Between the four arrays, there are some minor layout variations. The column outputs of each array are multiplexed into a PGA with 8x, 16x and 24x gain, and then the PGA output is driven by a source follower to the output pad. Digital

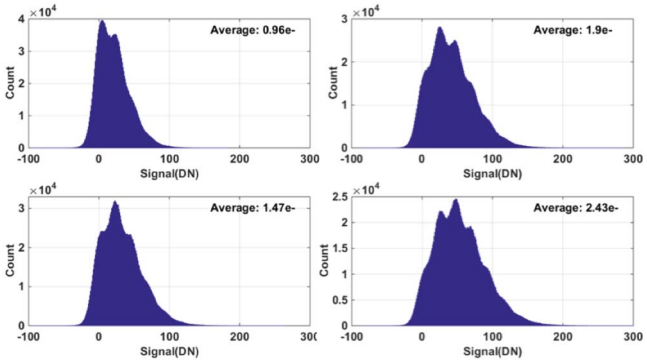

FIGURE 5. Photon Counting Histogram (PCH) for one SRO-jot with 0.42 e- r.m.s. read noise and 233μV/e- conversion gain. Each PCH is created from 2 million samples.

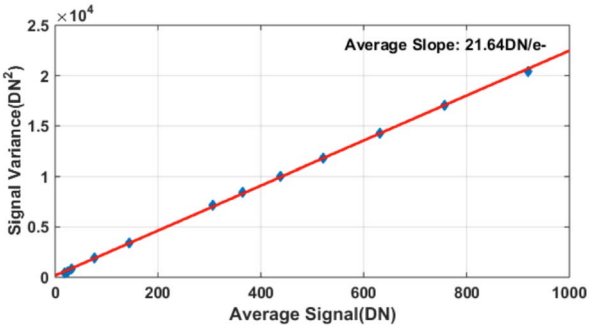

FIGURE 6. Photon Transfer Curve (PTC) of the jot array. The horizontal axis is the average of the signal in digital number (DN), and the vertical axis is the variance of the signal in the square of digital number (DN^2). Each data point on the curve is measured with the average of 200 frames. The slope of the PTC shows the average conversion gain (CG) is 21.64DN/e- after the in-jot source follower (SF), which is converted to 230.03μV/e-.

correlated double sampling (CDS) is done by an off-chip 14-bit ADC.

B. CG AND CG VARIATION

In the SRO jot arrays, the tapered reset transistor was not used to reduce risk, so compared to the TPG jots reported in [12], lower conversion gain is anticipated. In this jot, the major components of the FD capacitance are the FD junction capacitance, the RG overlap capacitance, the SF effective capacitance and the inter-metal capacitance. The TG overlap capacitance is eliminated by the PG structure. Comparing to the non-shared PG jot, the SRO jot has a more compact layout, so higher inter-metal capacitance is anticipated.

Some SRO jots showed mild quantization effect in their Photon Counting Histogram (PCH). As shown in Fig. 5, the SRO jots were illuminated by a LED light source, and one single SRO jot was readout 2,000,000 times under the same illumination level with 100μsec integration time. The PCH is the histogram of the 2,000,000 output signal samples. It should be noted that 2,000,000 samples are 10x more than what was used to create the PCHs for PG and TPG jots in [12], because more samples are required to create a smoother PCH when the read noise is higher than 0.4e- r.m.s.. Each sample was acquired from the jot with a single CDS and 10μsec CDS period. The Valley-Peak Modulation (VPM) showed the read noise of this jot is 0.42e- r.m.s., and the PCH peak-to-peak distance showed the CG is 233μV/e-.

Not all SRO jots had read noise lower than 0.45e- r.m.s., and PCH-VPM method couldn't be applied to characterize all the SRO jots. As discussed in [16], for photon-counting pixels the PCH and VPM can provide a more accurate measurement of CG and read noise. The PCH-VPM method works best when the read noise of pixels is below 0.45e- r.m.s. so the classic Photon Transfer Curve (PTC) method was used. The PTC of the SRO jot array is depicted in Fig. 6, each data point on the curve corresponds to the average signal and the square of the average noise from the SRO jot array under one illumination level, and each data point is averaged from 200 frames. The slope of the curve showed the average CG of the array is 230.0μV/e-, after in-jot SF, and 255.9μV/e- before in-jot SF.

Besides the PTC of the whole array, the PTC of each SRO jot was also analyzed so that CG variation could be measured. The relative standard deviation of jot CG is 3.7%. Theoretically, the CG of the four SRO-jots in each group should be exactly the same because the CG is determined by the FD capacitance. As expected, the four jots in each group have a smaller variation of 1.5%. This residual intra-group variation may be an artifact because the PTC method relies on the measurement of noise, and the accuracy of noise measurement needs a sufficiently large number of samples.

C. READ NOISE AND READ NOISE VARIATION

As mentioned in the last section, the PCH-VPM method cannot be applied to all the SRO jots, so the traditional dark measurement method was used to measure the total noise of each jot device. The 32x32 jot array has an average read noise of 110μV r.m.s., which corresponds to 0.48e- r.m.s., and the relative standard deviation is 20%.

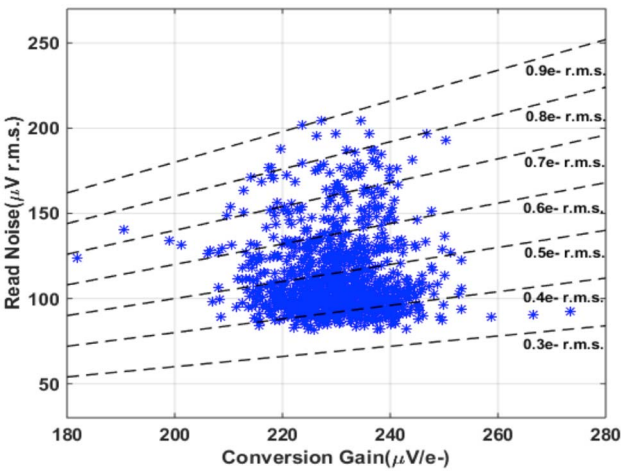

FIGURE 7. Scatter plot of read noise and conversion gain.

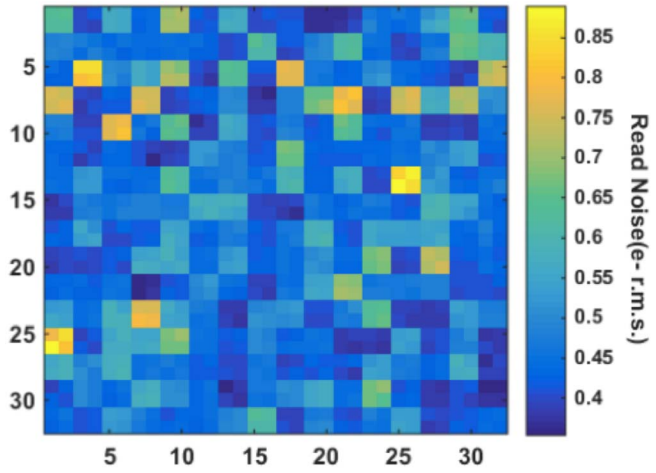

FIGURE 8. **The color-map of read noise of the 32x32 jot array. The average read noise is 0.48e- r.m.s., or 110μV r.m.s., and the relative standard deviation of read noise is 20%.**

A read noise vs. CG scatter plot is shown in Fig. 7, in which the vertical axis is read noise in μV r.m.s., while the horizontal axis shows CG in μV/e-. The dashed lines show constant read noise levels in e- r.m.s.. Similar to the CG, we expect the four jots in one group to have the same read noise, but small variation is observed in the results. A read noise color-map is depicted in Fig. 8. Possibly this is a result of low frequency noise components, such as RTS and FD dark current.

Read noise is the key factor of the photon counting capability, and with our approach, the low read noise is achieved by low FD capacitance. Some FD capacitance reduction techniques, such as tapered reset transistor and punch-through reset, were not applied to this SRO jot when this chip was designed to reduce the risk, but those techniques will be applied to our next generation SRO jots.

D. DARK CURRENT AND IMAGE LAG

Thanks to the potential barrier created by the PB region in a pump gate structure, the SW is well protected from the dark current generated near the surface interface, and the PG jot devices have very low SW dark current, as reported in [12]. A similar low dark current is observed in the SRO

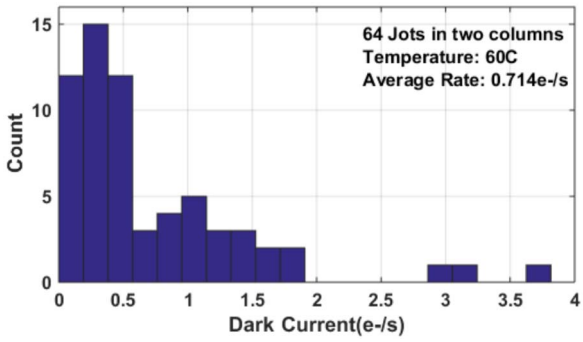

FIGURE 9. **The histogram of SW dark current from 64 jots in two columns at 60C. The average dark current per jot is 0.714e-/s, or 11.42pA/cm^2.**

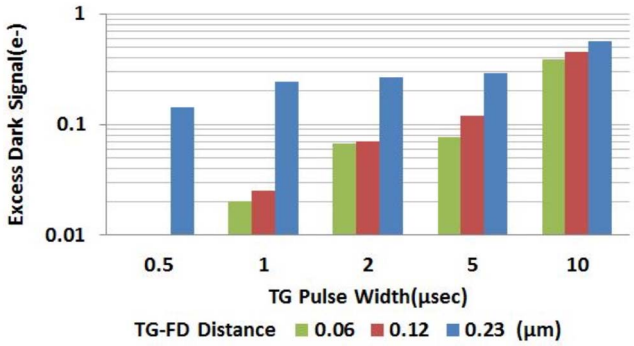

FIGURE 10. **The excess dark current changes with the TG pulse width and the TG-FD distance, measured with non-shared PG jots. The excess dark current becomes zero when the TG pulse width is shorter than 2μsec with the TG-FD distance shorter than 0.12μm.**

jots. At 60C, the average SW dark current is 0.714e-/s, or 11.42 pA/cm^2. The histogram of dark current is shown in Fig. 9. In [12], an excess dark current is also reported, which is generated only when TG is positively biased, and is proportional to the TG pulse width and the positive bias voltage. It was discovered that this excess dark current is also related to the TG-to-FD distance. As mentioned in [14], the pump gate structure aims to create a distal FD which has no overlap with TG to eliminate the overlap capacitance between TG and FD. And a very lightly doped p-type region VB is used to separate TG and FD. We found that the excess dark current increases monotonically with TG-FD distance, as shown in Fig. 10. One possible explanation for the excess dark current is that it is the thermal dark generation in the VB region. When TG is "on", according to the simulation, the VB region is fully depleted, and the dark generation rate in VB is greatly increased when it is fully depleted. With smaller TG-FD distance or lower TG "on" voltage, the area size of the fully depletion region is smaller, and with a TG-FD distance shorter than 0.12μm and a TG pulse width shorter than 2μsec, the excess dark current can be reduced to a negligible level. On the other hand, according to our PTC measurements for PG jot arrays with different TG-FD distance, the distance of 0.06μm or 0.12μm will not introduce more overlap capacitance or reduce CG. An even shorter TG-FD will eventually increase the FD total capacitance and reduce CG, but since 0.06μm is already the minimum variation in our design, the limit cannot be tested and the limit should also be process dependent. In a 1Mjot QIS, the TG pulse width is expected to be less than 500nsec with 1,000fps, and in a 1Gjot QIS, the TG pulse width will be even shorter, so the excess dark current will be negligibly low for QIS application with TG-FD distance of 0.12μm.

Lag was checked by pulsed illumination. In one cycle, jots were illuminated for 5 frames and not illuminated for the next 5 frames. The signal of one array of jots is accumulated over 1000 cycles, and a mean signal is calculated for each frame position. The result for SRO jots is shown in

Fig. 11 (top). Since all the SRO jots have a TG-FD distance of 0.23μm, an excess dark current of 0.3e- still exists in the dark frames. Since the signal in dark frames consists of the excess dark current and the lag, the lag should be the difference of the total residual signal from frame #6 to frame #10. Under this assumption, the observed lag is 0.05e- when the mean exposure signal is 14.6e-. This assumption was checked with non-shared PG jots with 0.12μm TG-FD distance. The result of the same test is shown in Fig. 11 (bottom). As expected, the excess dark current is negligible in the dark frames, and the lag is less than 0.01e- with an illumination of 10e-. According to this result, the SRO jots have relatively low lag but still higher than the non-shared PG jots. This may be caused by the different shape of TGs in the two kinds of jots, and the 3D effect creates small potential barrier underneath the TG in the SRO jots. Both the TG threshold adjustment doping and the TG-FD distance will be optimized for future SRO jot device to further reduce lag.

E. QUANTUM EFFICIENCY

The quantum efficiency (QE) of green light (550nm) was checked with a green LED. A calibrated light meter was used to measure the external intensity of the incident light at the plane where the sensor was located. Then, the total number of incident photons was calculated based on the green photon energy, the integration time (100μsec), and the jot area size. The QE was measured as the ratio between the number of photons collected by the jot device over the total incident photons. The QE of SRO jots is 65%, which shows a significant potential advantage over the non-shared PG jots, which showed a 40% QE at 550nm. Since the SRO jots used the same back-end process as the non-shared jots, we expect the difference in QE to be mainly caused by post-generation loss of carriers in silicon. The internal loss of photoelectrons is likely the result of the carriers collected by FD and other transistor terminals, such as the reset drain and source follower drain, and possibly some recombination. The loss of photoelectrons to FD was investigated by looking at the FD voltage change before and after a relative long integration time (600μsec) and comparing it with the signal accumulated in SW. It was found that in the non-shared PG jots, the amount of photoelectrons collected by FD is about 1/6 of that collected by SW, which reduced the effective QE of non-shared PG jots. But in SRO jots, since the 2X2 structure creates a better potential profile to deflect photons from FD, this proportion becomes as low as 1/100. It should be noted that all the jot devices used the TSMC standard back-end process, but microlens is not used. With microlens, the QE would be slightly improved. On the other hand, the doping of the deep SW nwell would need to be optimized in the future to improve blue light QE. In principle, the QE of jot devices can be as high as the QE of the best CIS.

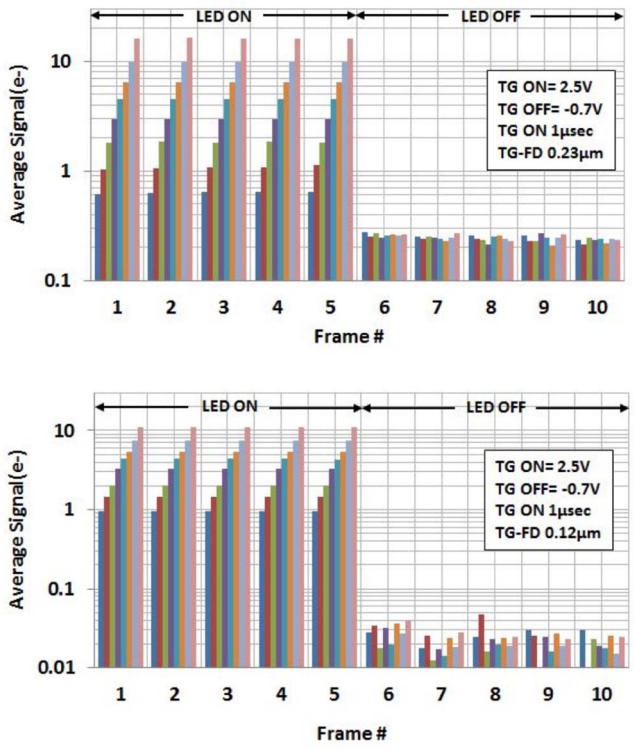

FIGURE 11. **Lag measurement for SRO jots (top) and non-shared PG jots (bottom) for 5 illuminated followed by 5 dark frames. The vertical axis means the average signal of each frame. Each frame set represents 8 different illumination levels. Note the change in scale for the compared results.**

TABLE 1. **SRO jot characterization results.**

	SRO jots
Pitch Size	1.0um
SF Size	0.4um x 0.2um
Col. Bias Current	416nA
PTC CG	230μV/e-
CG Variation	3.7%
Read Noise	0.48e- r.m.s.
Read Noise Std. Dev.	20%
SF 1/f noise	110μV r.m.s.
Dark Current @ 60C	0.71e-/s ($11.4\ pA/cm^2$)
Lag @ RT	<0.12e-
Full Well Capacity	250e-
QE @ 550nm	65.3%

IV. CONCLUSION

A 1μm-pitch pump-gate jot device with a 4-way shared readout structure is reported. Some major challenges in pixel/jot shrink are discussed, such as quantum efficiency and cross-talk. The crosstalk performance of this device was investigated with TCAD simulation and the actual device was characterized for conversion gain, read noise, dark current, lag and quantum efficiency. The results are listed in Table 1.

ACKNOWLEDGMENT

The authors appreciate the fabrication work done by TSMC led by H. Y. Cheng, Forza Silicon for use of their facilities during the design phase, and the technical assistance of other members of our group at Dartmouth, especially S. Chen and D. Hondongwa.

REFERENCES

[1] E. R. Fossum and D. B. Hondongwa, "A review of the pinned photodiode for CCD and CMOS image sensors," *IEEE J. Electron Devices Soc.*, vol. 2, no. 3, pp. 33–43, May 2014.

[2] E. R. Fossum, "What to do with sub-diffraction-limit (SDL) pixels? A proposal for a gigapixel digital film sensor (DFS)," in *Proc. IEEE Workshop CCDs Adv. Image Sensors*, Karuizawa, Japan, Sep. 2005, pp. 214–217.

[3] E. R. Fossum, "The quanta image sensor (QIS): Concepts and challenges," in *Proc. Opt. Soc. Amer. Topical Meeting Comput. Opt. Sens. Imag.*, Toronto, ON, Canada, Jul. 2011.

[4] N. Teranishi, "Required conditions for photon-counting image sensors," *IEEE Trans. Electron Devices*, vol. 59, no. 8, pp. 2199–2205, Aug. 2012.

[5] E. R. Fossum, "Modeling the performance of single-bit and multi-bit quanta image sensors," *IEEE J. Electron Devices Soc.*, vol. 1, no. 9, pp. 166–174, Sep. 2013.

[6] R. Zizza, "Jots to pixels: Image formation options for the quanta image sensor," M.S. thesis, Thayer School Eng., Dartmouth College, Hanover, NH, USA, 2015.

[7] M. R. Guidash, "Shared amplifier pixel with matched coupling capacitances," U.S. Patent WO2 006 130 519 A2, Dec. 7, 2005.

[8] J.-C. Ahn *et al.*, "7.1 a 1/4-inch 8Mpixel CMOS image sensor with 3D backside-illuminated 1.12μm pixel with front-side deep-trench isolation and vertical transfer gate," in *Proc. ISSCC*, San Francisco, CA, USA, 2014, pp. 124–125.

[9] D. N. Yaung *et al.*, "High performance 300mm backside illumination technology for continuous pixel shrinkage," in *Proc. Int. Electron Devices Meeting (IEDM)*, Washington, DC, USA, Dec. 2011, pp. 8.2.1–8.2.4.

[10] Y. Kitamura *et al.*, "Suppression of crosstalk by using backside deep trench isolation for 1.12μm backside illuminated CMOS image sensor," in *Proc. Int. Electron Devices Meeting (IEDM)*, San Francisco, CA, USA, Dec. 2012, pp. 24.2.1–24.2.4.

[11] J. Ma and E. R. Fossum, "Quanta image sensor jot with sub 0.3e- r.m.s. read noise and photon counting capability," *IEEE Electron Device Lett.*, vol. 36, no. 9, pp. 926–928, Sep. 2015.

[12] J. Ma, D. Starkey, A. Rao, K. Odame, and E. R. Fossum, "Characterization of quanta image sensor pump-gate jots with deep sub-electron read noise," *IEEE J. Electron Devices Soc.*, vol. 3, no. 6, pp. 472–480, Nov. 2015.

[13] M.-W. Seo *et al.*, "A 0.27e^-_{rms} read noise 220-μV/e^- conversion gain reset-gate-less CMOS image sensor with 0.11-μm CIS process," *IEEE Electron Device Lett.*, vol. 36, no. 12, pp. 1344–1347, Dec. 2015.

[14] J. Ma and E. R. Fossum, "A pump-gate jot device with high conversion gain for a quanta image sensor," *IEEE J. Electron Devices Soc.*, vol. 3, no. 2, pp. 73–77, Mar. 2015.

[15] Y. Huo, C. C. Fesenmaier, and P. B. Catrysse, "Microlens performance limits in sub-2μm pixel CMOS image sensors," *Opt. Exp.*, vol. 18, no. 6, pp. 5861–5872, Mar. 2010.

[16] D. Starkey and E. R. Fossum, "Determining conversion gain and read noise using a photon-counting histogram method for deep sub-electron read noise image sensors," submitted for possible publication to *IEEE J. Electron Devices Soc.*, Dec. 2015.

JIAJU MA (S'12) received the B.S. degree in applied physics from Nankai University, Tianjin, China, in 2012. He is currently pursuing the Ph.D. degree with the Thayer School of Engineering, Dartmouth College. His research focus is developing and characterizing the quanta image sensor (QIS) and the QIS jot device, with emphasis on the jot device TCAD modeling and the jot device fabrication process design.

LEO ANZAGIRA (S'11) received the B.A. degree in engineering sciences and the B.E. degree in electrical engineering from Dartmouth College, in 2011, where he is currently pursuing the Ph.D. degree with the Thayer School of Engineering. He was an Intern with Forza Silicon Corporation and Aptina Imaging Corporation. His research interests include low light color imaging, 3-D time-of-flight imaging, and color image processing.

ERIC R. FOSSUM (S'80–M'84–SM'91–F'98) is currently a Professor with the Thayer School of Engineering, Dartmouth College. He is the primary inventor of the CMOS image sensor used in billions of camera phones and other applications. He was inducted into the National Inventors Hall of Fame. He is currently exploring the Quanta Image Sensor. He is the Co-Founder and the Past President of the International Image Sensor Society and the Director of the National Academy of Inventors. He is a member of the National Academy of Engineering.